

MedMAP: Promoting Incomplete Multi-modal Brain Tumor Segmentation with Alignment

Tianyi Liu, Zhaorui Tan, Muyin Chen, Xi Yang, Haochuan Jiang, Kaizhu Huang

Abstract—Brain tumor segmentation is often based on multiple magnetic resonance imaging (MRI). However, in clinical practice, certain modalities of MRI may be missing, which presents a more difficult scenario. To cope with this challenge, Knowledge Distillation, Domain Adaption, and Shared Latent Space have emerged as commonly promising strategies. However, recent efforts typically overlook the modality gaps and thus fail to learn important invariant feature representations across different modalities. Such drawback consequently leads to limited performance for missing modality models. To ameliorate these problems, pre-trained models are used in natural visual segmentation tasks to minimize the gaps. However, promising pre-trained models are often unavailable in medical image segmentation tasks. Along this line, in this paper, we propose a novel paradigm that aligns latent features of involved modalities to a well-defined distribution anchor as the substitution of the pre-trained model. As a major contribution, we prove that our novel training paradigm ensures a tight evidence lower bound, thus theoretically certifying its effectiveness. Extensive experiments on different backbones validate that the proposed paradigm can enable invariant feature representations and produce models with narrowed modality gaps. Models with our alignment paradigm show their superior performance on both BraTS2018 and BraTS2020 datasets.

Index Terms—Brain Tumor Segmentation, Missing Modality, Modality Gap, Multi-modal Segmentation, Alignment,

I. INTRODUCTION

BRAIN tumors pose severe risks to human life, making precise medical segmentation essential as it devises effective treatment planning and strategies [1]. Brain tumor

Tianyi Liu is with the University of Liverpool and School of Robotics, XJTLU Entrepreneur College (Taicang), Xi'an Jiaotong-Liverpool University; Zhaorui Tan is with the University of Liverpool and School of Advanced Technology, Xi'an Jiaotong-Liverpool University; Muyin Chen and Haochuan Jiang are with the School of Robotics, XJTLU Entrepreneur College (Taicang), Xi'an Jiaotong-Liverpool University; Xi Yang is with School of Advanced Technology, Xi'an Jiaotong-Liverpool University; Kaizhu Huang is with Data Science Research Center, Duke Kunshan University

The work was partially supported by the following: National Natural Science Foundation of China under No.92370119, No. 62206225, and No. 62376113; Jiangsu Science and Technology Program (Natural Science Foundation of Jiangsu Province) under No. BE2020006-4; Natural Science Foundation of the Jiangsu Higher Education Institutions of China under No. 22KJB520039; XJTLU Research Development Funding 20-02-60. Computational resources used in this research are provided by the School of Robotics, XJTLU Entrepreneur College (Taicang), Xi'an Jiaotong-Liverpool University.

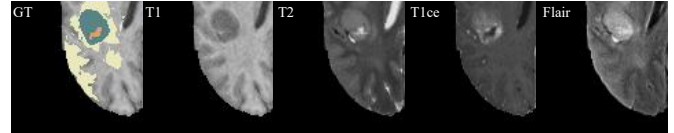


Fig. 1: Images of the four modalities in the brain tumor dataset with the ground truth (GT) segmentation label. Different colors represent different organs: Orange: NCR/NET, Yellow: ED, and Blue: ET.

segmentation methods usually employ Multiple Magnetic Resonance Imaging (MRI) visualizations, including Fluid Attenuation Inversion Recovery (Flair), contrast-enhanced T1-weighted (T1ce), T1-weighted (T1), and T2-weighted (T2), as illustrated in Figure 1, as multiple modalities [2]. Particularly, the aforementioned modalities complement each other to understand both the physical structure and physiopathology of tumors; their combination naturally leads to improved segmentation performance [3]–[6]. For instance, T2 and Flair imaging modalities are valuable for assessing the enhanced tumor (ET), whereas T1 and T1ce modalities are effective in delineating the core of the tumor, including the necrotic, non-enhancing, and enhancing regions (NCR/NET) [7]. However, not all modalities are always available in real clinical practice due to scenarios such as data corruption and/or variations in scanning protocols, leading to crucial challenges of developing a generalized multi-modal approach that copes with the absence of certain modalities [8]–[11].

In response to the challenge of missing modalities, previous substantial efforts have converged on two primary strategies: Knowledge Distillation (KD), and Domain Adaptation (DA). The KD-based attempts involve transferring the knowledge from the complete multi-modality teacher to the incomplete missing-modality student [1], [12]–[14], while the methods in DA leverage alignment methods to bridge the gap between the model trained on complete modalities and those trained on incomplete ones [15]. However, these two strategies ignore gaps existing between the modalities as they often process different modalities as separate channels, leading to a failure to capture the important invariance across modalities. To better alleviate the modality gaps, another branch of methods, named Shared Latent Space (SLS), transfers each modality into a common representation space shared among all modalities [7], [16]–[18]. It argues that they can learn the inter-modality invariance [18], but the detailed analysis of minimized modality

gaps seems missing. As illustrated in Figure. 2, we reveal that the modality gaps still exist in most previous methods. Particularly, SLS-based methods have been observed to alleviate the modality gaps, but these gaps have not been sufficiently eliminated.

This paper mainly studies the critical but an under-explored question for missing modality segmentation: Can minimizing modality gaps improve the model’s generalization and lead to better missing modality performance? Our extensive experiments unveil that minimizing modality gaps leads to consistent improvements in various missing modalities approaches, including those following KD, DA, and SLS strategies. Furthermore, to achieve a convincing minimization of modality gaps for different approaches, we propose the **Medical Modality Alignment Paradigm (MedMAP)**, which is feasible for most existing missing modality approaches.

The design of MedMAP is inspired by minimizing domain gaps for natural visual segmentation [19], [20], which consistently yields improvements across various approaches and often relies on pre-trained models trained by abundance data. Specifically, the distribution of latent features from the pre-trained model is used as the alignment anchor to minimize domain gaps, providing stable and reliable alignment guidance. However, promising pre-trained models for medical tasks, especially brain tumor segmentation tasks, are often unavailable due to a lack of data.

To tackle this issue, MedMAP includes a pre-defined distribution, P_{mix} , as the substitution of the pre-trained model. Especially, MedMAP incorporates a feature-encoding pipeline \mathcal{T} to map the latent features of different modalities into a shared space, and the latent distributions of these modalities are aligned to the pre-defined P_{mix} . Theoretically, we show that individually aligning each modality to P_{mix} in MedMAP achieves better performance than mapping them collectively to P_{mix} , reducing the modality gaps in a better manner that benefits the downstream prediction tasks in missing-modality scenarios. Besides, the efficacy of MedMAP with two concrete proposed forms of P_{mix} is empirically validated with different approaches. Extensive experimental results demonstrate that MedMAP can reduce the modality gap and yield substantial benefits in a range of medical tasks where different modalities are absent. The major contributions of the paper are summarized as follows:

- We proposed a pre-defined distribution P_{mix} , which is part of the **Medical Modality Alignment Paradigm (MedMAP)**, as the substitution of the pre-trained model in the missing modality scenario.
- We provide theoretical support for our MedMAP, showing that individually aligning each modality to P_{mix} certifies tighter Evidence Lower Bound than mapping all modalities as a whole to P_{mix} .
- We empirically verify the effectiveness of our MedMAP in enhancing brain tumor segmentation performance when using the latest state-of-the-art backbones in scenarios where certain modalities are missing. It substantially mitigates modality gaps and properly learns the cross-modality invariance.

The rest of this article is organized as follows. Section II

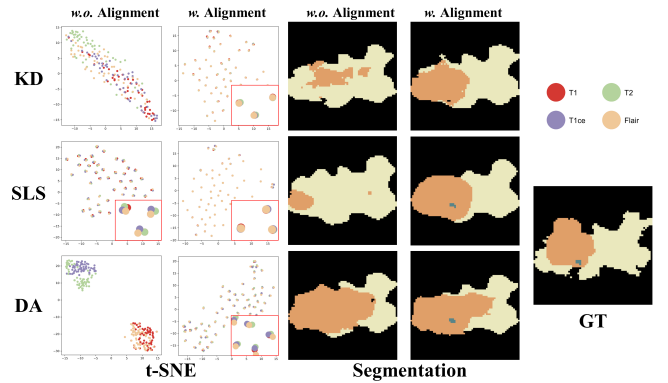


Fig. 2: T-SNE and segmentation visualization of different strategies with (*w.*) and without (*w.o.*) alignment. Different colors in t-SNE represent different modalities. GT denotes the groundtruth label.

reviews related works on brain tumor segmentation with incomplete modalities. Section III provides the theoretical motivations of our alignment paradigm. Section IV describes the alignment paradigm in detail. We evaluate our alignment paradigm with state-of-the-art methods and provide the ablation studies in Section V. The article is concluded in Section VII.

II. RELATED WORK

A. Multi-modal Learning for Missing Modalities

Flair, T1, T2, and T1ce are complementary modalities utilized to segment brain tumors [2]. Segmentation performance unfortunately drops drastically in the scenario when some modalities are missing due to practical difficulties such as data corruption and/or scanning protocol variations [8]–[11], [21]. Prior arts have proposed several methods to deal with the missing modality problem, which can be generally divided into three categories: Knowledge Distillation, Share Latent Space, and Domain Adaption.

Knowledge Distillation (KD) based approaches transfer knowledge from teachers with complete modality information to students with missing modality information. In [1], Kullback-Leibler (KL) loss and an additional contrastive loss are engaged to guide the student to imitate soft distributed features from the teacher and reduce latent space divergence between them respectively. ProtoKD [13] employs a prototype knowledge distillation loss to encourage simultaneous intra-class concentration and inter-class divergence. In these methods, students’ performance is always based on teachers’ performance. However, students often lead to sub-optimal segmentation performance since their teachers do not consider the feature invariant information and domain-specific information among those modalities.

Shared Latent Space (SLS) methods retrieve missing information by exploiting the multimodal latent feature space. RFnet [7] uses different encoders to extract the modality-specific information and a decoder to share the weights for those modalities to build a shared representation. Different modality features are fused at different levels. MmFormer [18]

introduces Transformers to exploit intra- and inter-modality dependency for feature fusion. These methods presume that there are no modality gaps among these modality features and fuse them directly. They consider modality-invariant information yet ignore modality-specific information.

Domain Adaptation (DA) based methods aim to minimize the gap between complete modality models and incomplete models as they share different domains. Adversarial Co-training Network (ACN) [15] consists of a multimodal path (to obtain rich modality information) and a unimodal path (to generate modality-specific feature representations). Then, a co-training approach is introduced to establish a coupled learning process between them. However, although ACN narrows the gaps between complete and incomplete modality models, it still ignores the gaps between different modalities within complete modality models.

This paper reveals that all the aforementioned methods are influenced by the knowledge acquired by the base model, and mitigating the modality gaps in the base model benefits all of them. To address this, we uniformly summarize the mathematical forms of these methods in Section III-A to validate this issue.

B. Alignment in Multi-domain Generalization

Gaps in the latent space arise not only across various modalities but also span across distinct data domains. To address the domain generalization task, many attempts have been made towards a narrowed gap. For instance, recent efforts [22]–[25] learn domain-independent representations by reducing the gaps to improve generalization to classify images, which are, however, not directly applicable to semantic segmentation. In our research, we borrow the idea from the domain generalization to perform proper alignment between latent distributions in the *teacher*. To this end, we successfully reduce the modality gaps to overcome the difficulty of missing modality, thereby improving the segmentation of the medical image in all categories.

III. THEORETICAL MOTIVATION

In this section, we underscore the significance of reducing modality gaps that prior methodologies have overlooked. We present the problem formulations for three distinct types of approaches and illustrate the enhancement of domain alignment through the strategic use of P_{mix} . Furthermore, we explore different techniques for deriving practical empirical representations of P_{mix} .

Notations. We denote the model, i.e., the teacher model for knowledge distillation, the model for shared latent space, or the model pretrained for domain adaptation as the base model. Considering J as the number of the set of modalities of medical images with paired observations and targets $\{\mathbf{X}_j, \mathbf{Y}_j\}_{j=1}^J$ from the modality j . Note for medical modalities, \mathbf{Y} remains static for all modalities. The encoders of the base model are denoted as $\mathcal{T} : \mathcal{T}(\mathbf{X}_j) \rightarrow \mathbf{Z}_j^*$ where \mathbf{Z}_j^* denotes the latent feature obtained from the base model of the j^{th} modality. Simultaneously, a predictor \mathcal{C} that predicts segmentation masks from $\{\mathbf{Z}_j^*\}_{j=1}^J$ as $\mathcal{C}^* : \mathcal{C}^*(\{\mathbf{Z}_j^*\}_{j=1}^J) \rightarrow \mathbf{Y}$. Correspondingly,

we denote the possible downstream model, e.g., the student models for knowledge distillation and the adapted model for the domain adaptation, for the j^{th} target modality as $\mathcal{S}_j : \mathcal{S}_j(\mathbf{X}_j) \rightarrow \mathbf{Z}_j$ of each modality with their predictor $\mathcal{C}_j : \mathcal{C}(\mathbf{Z}_j) \rightarrow \mathbf{Y}$. Let $P(\cdot)$, $D_{KL}(\cdot\|\cdot)$, $H(\cdot)$, $H_c(\cdot, \cdot)$, $I(\cdot; \cdot)$ denote the probability of a random variable from the distribution, Kullback–Leibler divergence, entropy, cross-entropy, and mutual information respectively.

A. Previous Methods

Despite the various approaches adopted to handle missing modalities, the common strategy involves training a base model \mathcal{T} that retains information from all modalities as its foundation. Therefore, the objective for training \mathcal{T} can be summarized as:

$$\max_{\mathcal{C}^*} \sum_{j=1}^J \mathbb{E}_{\mathbf{Z}_j^* \sim P(\mathbf{Z}_j^*)} [\ln P(\mathbf{Y} | \mathcal{C}^*(\mathbf{Z}_j^*))] + \zeta, \quad (1)$$

where ζ denotes any possible regularization. Eq. 1 can be changed in the form of information entropy as:

$$\min_{\mathcal{C}^*} \sum_{j=1}^J H_c(P(\mathcal{C}^*(\mathbf{Z}_j^*)), P(\mathbf{Y})) + \zeta. \quad (2)$$

The base model can be adapted for different downstream approaches under the missing modality scenario. We provide details for each type of missing modality approaches as follows:

KD. In knowledge distillation for medical segmentation with missing modality, the process involves two main steps: training the teacher and student models. As previously mentioned, the teacher model is denoted as the base model \mathcal{T} ; its objective is in the form of Eq. 1. Notably, previous methods [1], [12], [13] uses no extra regularization for training \mathcal{T} , i.e., $\zeta_{KD} := 0$. Meanwhile, for one possible student model \mathcal{S}_j encoder and \mathcal{C}_j classifier trained with missing modalities that leverages knowledge from \mathcal{T} , its objective is:

$$\max_{\mathcal{S}_j, \mathcal{C}_j} \mathbb{E}_{\mathbf{Z}_j \sim P(\mathbf{Z}_j)} [\ln P(\mathbf{Y} | \mathcal{C}_j(\mathbf{Z}_j))] - D_{KL}(P(\mathcal{S}_j(\mathbf{X}_j)) \| P(\mathbf{Z}_j^*)). \quad (3)$$

SLS. For approaches aiming to achieve better-fused representations from a shared latent space of all modalities, the focus is on enhancing the fusion mechanism of \mathcal{T} through additional losses and modifications to model architectures, denoted as ζ_{SLS} . However, it is important to note that the current shared latent space ζ_{SLS} methods often do not adequately address the mitigation of modality gaps.

DA. Domain adaptation methods address modality gaps by continually adapting the base model \mathcal{T} through specific training with missing modality settings. Considering a possible adaptation \mathcal{S}_j encoder and \mathcal{C}_j classifier derived from \mathcal{T} trained with missing modalities, its objective can be simplified as:

$$\max_{\mathcal{S}_j, \mathcal{C}_j} \mathbb{E}_{\mathbf{Z}_j \sim P(\mathbf{Z}_j)} [\ln P(\mathbf{Y} | \mathcal{C}_j(\mathcal{S}_j(\mathbf{X}_j)))]. \quad (4)$$

Limitations. Albeit their impressive results, most existing methods in the mentioned categories share a common limitation: they often disregard the potential modality gap in \mathcal{T} , which can hinder the performance of missing modality tasks.

Consider a real-valued convex loss $L(\theta)$ where θ denotes any possible model; the empirical risk [26] introduced by the model θ for methods without considering the modality gap can be written as

$$\int L(Z_j^*, Y_j) dP(\theta) + \mathbb{E}_{i,j=1}^J D_{KL}(P(Z_i^*) \| P(Z_j^*)). \quad (5)$$

This equation indicates that extra risks would be introduced by the possible modality gaps, thus causing performance degradation. Therefore, our approach is based on minimizing the gap across modalities in latent space while maintaining the prediction performance of the latent features.

B. Aligning Medical Multi-modalities

This section explores an innovative strategy designed to bridge the modality gap, specifically for the base model \mathcal{T} . We also demonstrate that our approach can improve many methods across all three categories.

Minimizing modality gap improve generalization ability of the \mathcal{T} . In the context of domain generalization, minimizing the modality gap can be interpreted as reducing the distributional discrepancy between the source domain S and the target domain T as [27]:

$$\epsilon_T(h) \leq \epsilon_S(h) + d_{H\Delta H}(S, T) + \lambda \quad (6)$$

where $\epsilon_T(h)$ is the error rate of the model on the target domain, $\epsilon_S(h)$ is the error rate of the model on the source domain, $d_{H\Delta H}(S, T)$ is the distributional discrepancy between the source and target domains, and λ is a term related to the complexity of the hypothesis space.

Reducing the distributional discrepancy between the source and target domains, thereby reducing $d_{H\Delta H}(S, T)$, which theoretically lowers the error rate on the target domain and thus improves the model's generalization ability. In the modality generalization tasks, reducing $d_{H\Delta H}$ of different modalities can also improve the model's generalization ability.

How to align to the pre-defined anchor P_{mix} . Assuming that there is a feasible P_{mix} in the latent space which preserves the prediction performance, i.e., the minimization of $\int L(Z_j^*, Y_j) dP(\theta)$ in Eq. 5 is guaranteed, minimization of Eq. 5 can be changed as:

$$\min D_{KL}(P(\mathbf{Z}_j^*) \| P_{mix}) + H_c(P(\mathcal{C}^*(\mathbf{Z}_j^*)); P(\mathbf{Y})). \quad (7)$$

To derive an empirical form of minimizing the term $D_{KL}(P(\mathbf{Z}_j^*) \| P_{mix})$, we first introduce Proposition 1:

Proposition 1: For training a multi-modal *teacher* model, it is assumed that the existence of one modality \mathbf{Z}_i is independent of the other modality \mathbf{Z}_j where $i \in \{1, \dots, J\}, j \in \{1, \dots, J\}, i \neq j$. In other words, if one modality is missing or corrupted, other modalities can still exist. In this scenario, there exists a probability distribution P_{mix} that can be used as an anchor distribution to align the latent variables \mathbf{Z}^* , while preserving sufficient information for accurate prediction of the segmentation labels \mathbf{Y} .

Proof: The modality existence independent assumption is derived from the fact that each modality is independent of each other. If P_{mix} preserves sufficient information for accurate

prediction of the segmentation labels \mathbf{Y} , based on the joint and marginal mutual information, we have

$$\sum_{j=1}^J I(P_{mix}(\mathbf{Z}_j^*); P(\mathbf{Z}_j^*)) \leq I(P_{mix}(\mathbf{Z}^*); P(\mathbf{Z}^*)). \quad (8)$$

Eq. 8 shows that individually mapping each modality \mathbf{Z}_j^* to P_{mix} is a lower bound of mapping all modalities together to P_{mix} . ■

Proposition 1 is **single-letterization** that simplifies the optimization problem over a large-dimensional (i.e., multi-letter) problem. Therefore, we individually align representations of each modality to the anchor P_{mix} rather than the whole distribution of all representations from all modalities. Furthermore, the former term of Eq. 8 can be derived as:

$$\sum_{j=1}^J \mathbb{E}_{\mathbf{Z}_j^* \sim P(\mathbf{Z}_j^*)} [\ln P(\mathbf{Y} | \mathcal{C}^*(\mathbf{Z}_j^*)) - D_{KL}(P(\mathbf{Z}_j^*) \| P_{mix})], \quad (9)$$

while the latter term is reformed as:

$$\mathbb{E}_{\mathbf{Z}^* \sim P(\mathbf{Z}^*)} [\ln P(\mathbf{Y} | \mathcal{C}^*(\mathbf{Z}^*)) - D_{KL}(P(\mathbf{Z}^*) \| P_{mix})]. \quad (10)$$

Eq. 9 presents the Evidence Lower Bound (ELBO) and we have Eq. 9 \leq Eq. 10 which indicates that Eq. 9 is tighter than the latter. Thus, instead of minimizing the gap between all modalities and P_{mix} , the alternative objective for \mathcal{T} is derived from Eq. 9 as:

$$\min \sum_{j=1}^J [D_{KL}(P(\mathbf{Z}_j^*) \| P_{mix}) + H_c(P(\mathcal{C}^*(\mathbf{Z}_j^*)); P(\mathbf{Y}))]. \quad (11)$$

As shown in Eq. 11, the essential point is finding a feasible P_{mix} that anchors all latent features in the space while preserving the prediction ability from the latent features to targets for all downstream adaptations. We introduce possible forms of P_{mix} as follows.

Possible approximations of pre-defined anchor P_{mix} . The selection of P_{mix} is critical for MedMAP and may vary across different base model backbones. Thus, instead of manual selection, we empirically determine that the optimal P_{mix} is a weighted mixture of all modalities' latent feature distributions. Specifically, $P_{mix}^* \triangleq \sum_{j=1}^J w_j P(\mathbf{Z}_j)$ where w_j is the associated weight of each modality. To validate P_{mix}^* , we compare it to two other possible empirical forms of P_{mix} : 1) Intuitive selection P_{mix}^k where a latent distribution of one modality is selected from $\{P(\mathbf{Z}_j^*)\}_{j=1}^J$ (i.e., $P_{mix}^k \triangleq P(\mathbf{Z}_{j=k}^*)$ where $k \in J$). 2) Assume that P_{mix} follows a normal distribution denoted as P_N . Extensive experiments in Section V demonstrate that using P_{mix}^* consistently yields improvements across different base model backbones under various missing modality settings. Validating P_{mix}^* 's superiority in comparison to P_{mix}^k and P_N .

IV. METHODOLOGY

A. Alignment Paradigm

MedMAP consists of a feature encoding pipeline and an anchor that latent space of the features will be aligned to. The encoder is a simple convolution that aims to map all the modality features into a shared latent space, so that alignment can be

applied. With the given P_{mix} , we align each modality latent features $\mathbf{Z}_{j,j \in \{1, \dots, J\}}^*$ to P_{mix} . By converting multi-modal features into a pre-defined distribution, we aim to standardize the scale and distributional properties of data originating from heterogeneous sources, thereby enabling cross-modal learning of distinctive features. In this article, two kinds of P_{mix} are proposed: P_{mix}^k and P_{mix}^* . We denote B, J , the batch size, and the number of modalities, respectively.

1) *Aligning to P_{mix}^k* : To derive P_{mix}^k , we first train the backbones using each modality independently and then evaluate the trained models over all modalities. We select the modality designated as the k^{th} modality, which is identified when the models demonstrate the superior performance when evaluated across j modalities. Following this, we define $P_{mix}^k \triangleq P(\mathbf{Z}_{j=k}^*)$. For aligning other modalities to the selected k^{th} modality, we minimize:

$$\mathcal{L}(\mathcal{T}) = \frac{1}{BJ} \sum_{b=1}^B \sum_{j=1}^J \|(z_j - z_k)\|^2, \quad (12)$$

where z are features of different modalities, $z_j \sim \mathbf{Z}_j$ are features that need to be aligned to $x_k \sim \mathbf{Z}_k$ from the k^{th} modality;

2) *Aligning to P_{mix}^** : In the quest to derive a more conducive latent space for integrating all modalities, we have advanced an innovative methodology termed Adaptive Alignment. This approach will transcend the basic alignment method that confines the latent space to a specific modality (P_{mix}^k). Adaptive Alignment operates under the presumption that an optimal latent space, termed as P_{mix}^* , for a prior modality can serve as a foundational anchor. Following this, we define $P_{mix}^* \triangleq \sum_{j=1}^J w_j P(\mathbf{Z}_j)$, where $w_j \in w = \{w\}_{i=i}^J$ are learnable weights. Then we minimize:

$$\mathcal{L}(\mathcal{T}, w) = \frac{1}{BJ} \sum_{b=1}^B \sum_{j=1}^J \left\| z_j - \sum_{j=1}^J w_j z_j \right\|^2, \quad (13)$$

where $x_j \sim \mathbf{Z}_j$ are features that need to be aligned, and $\sum_{j=1}^J w_j z_j$ is the adaptive anchor learned from all the features.

Unlike P_{mix}^k , P_{mix}^* does not rely on one specific pre-defined distribution. Such characteristic enables P_{mix}^* to more effectively adapt to various multi-modality datasets, requiring less prior knowledge.

B. Backbones

1) *KD*: As shown in Fig. 3a, in the KD methods, there are two branches: the teacher, and the student. Teacher models are trained with a full-modality dataset. Student models are trained with an incomplete-modality dataset and soft labels from the teacher model.

For training the teacher, each modality is encoded into a shared latent space and then aligned to the pre-defined P_{mix} . Specifically, as shown in Eq. 8, each modality representation is individually aligned to P_{mix} . The aligned features then become the input to the original teacher backbone. Therefore, the objective of training the teacher will be:

$$\mathcal{L}_{KD \text{ base}} = \mathcal{L}_{seg}^T + \alpha \mathcal{L}_A, \quad (14)$$

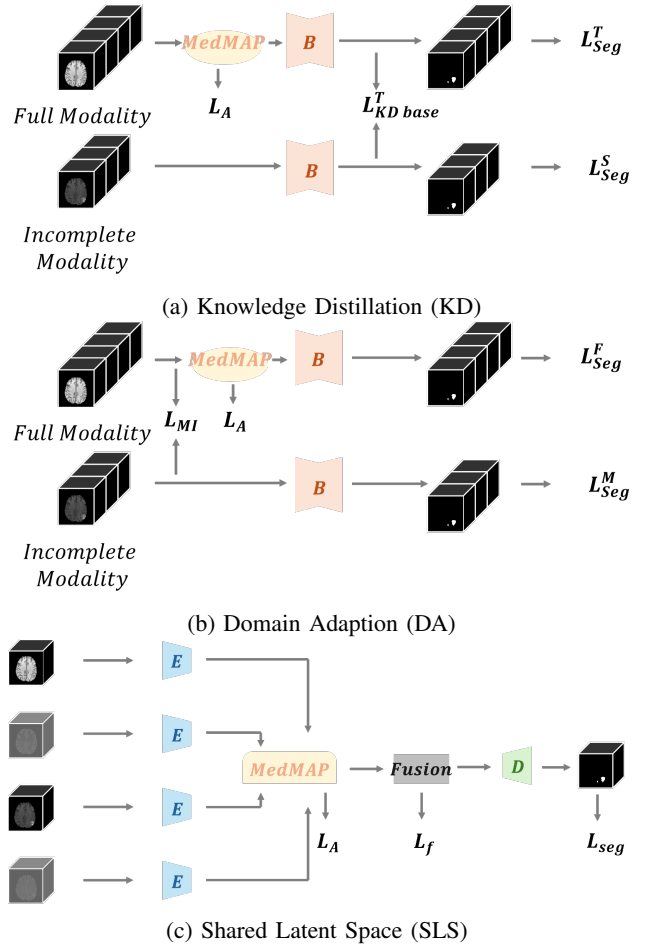


Fig. 3: Baseline architectures: a) KD, b) DA, c) SLS. B is the baseline model structure which represents 3D U-Net according to the baselines. E , fusion, and D are encoder, fusion, and decoder modules that compose SLS baseline architecture.

where \mathcal{L}_{seg}^T is the segmentation loss of teacher and \mathcal{L}_A is the alignment loss. α is a parameter which is empirically set to 0.125 in this work. Given that students harness the distilled knowledge from their teachers during training, their performance serves as a valuable indicator of teacher effectiveness. Therefore, we employ the student performance as a means to validate the feasibility of MedMAP for KD.

Specifically, the teacher model remains frozen, which preserves the integrity of the pre-learned representations and enables us to concentrate on assessing how effectively the student model can emulate the fixed knowledge rather than updating the teachers during student training. Consequently, the learning process of the student model is supported by the ground truth and the teacher's knowledge with the overall objective \mathcal{L} as:

$$\mathcal{L}_{KD} = \mathcal{L}_{seg}^S + \mathcal{L}_{KD \text{ base}}^T, \quad (15)$$

where \mathcal{L}_{seg}^S is the hybrid segmentation loss supervised by the hard labels of the student, and \mathcal{L}^T denotes the loss that receives supervision from the teacher.

2) *SLS*: As shown in Fig. 3c, SLS models always have a modality-specific encoder, a modality fusion encoder, and

a decoder [18]. In the modality-specific encoder, information within a specific modality will be extracted. The modality-fusion encoder will be used to create modality-invariant features with global semantics corresponding to the tumor region. A decoder is used to recover the information. We will align the well-extracted feature before the modality-specific encoder. Therefore, the total objective of SLS will be:

$$\mathcal{L}_{SLS} = \mathcal{L}_{seg} + \mathcal{L}_f + \alpha\mathcal{L}_A, \quad (16)$$

where \mathcal{L}_{seg} is the segmentation loss, \mathcal{L}_f is the possible fusion loss which has been proposed by the backbones; \mathcal{L}_A is the alignment loss, and α is a parameter which is empirically set to 0.125 in this paper.

3) *DA*: As shown in Fig. 3b, similar to KD, DA also has two branches: the full modality branch and the incomplete modality branch. It distills semantic knowledge by minimizing the Kullback-Leibler (KL) between the two branches. Meanwhile, besides the KL loss, it considers the domain gaps between the full modality model and the incomplete modality model. In ACN [15], it optimizes the hierarchical mutual information by minimizing the mutual information loss (\mathcal{L}_{MI}) between these two paths. We argue that we need not only consider the domain gap between the two branches, but also emphasize the domain gap among different modalities. Therefore, we add the MedMAP at the same place with \mathcal{L}_{MI} . It is noted that different from KD, DA is a co-training network. The full-modality model will not be frozen when training. Therefore, the whole objective will be:

$$\mathcal{L}_{DA} = \mathcal{L}_{seg}^{\mathcal{F}} + \mathcal{L}_{seg}^{\mathcal{M}} + \mathcal{L}_{MI} + \alpha\mathcal{L}_A, \quad (17)$$

where $\mathcal{L}_{seg}^{\mathcal{F}}$ and $\mathcal{L}_{seg}^{\mathcal{M}}$ are the segmentation loss of the full modality model and incomplete model respectively and \mathcal{L}_A is the alignment loss. α is a parameter which is also set to 0.125 empirically in this paper.

V. EXPERIMENT CONFIGURATIONS

A. Datasets

The BraTS datasets in 2018 and 2020 [4], [28], consisting of 285 and 369 subjects respectively, are employed for evaluation. Four individual modalities including T1, T1ce, T2, and Flair construct a specific subject, displaying brain tumor sub-regions *i.e.* enhancing tumor (ET), peritumoral edema (ED), and the necrotic and non-enhancing tumor core (NCR/NET). Specifically, each modality captures different properties of brain tumor sub-regions: GD-enhancing tumor (ET), peritumoral edema (ED), and the necrotic and non-enhancing tumor core (NCR/NET), nesting into three key segmentation targets, *i.e.*, whole tumor (WT, ET+ED+NCR/NET), tumor core (TC, ET+NCR/NET), and ET. For both datasets, we use Dice Score

TABLE I: Comparison of average Dice (%) on BraTS2018 and BraTS2020. w.o. is without, w. is with, Δ is an improvement.

Dataset	Models	PMKL [1] (KD)	mmFormer [18] (SLS)	ACN (DA) [15]
BraTS2018	w.o. MedMAP	65.44	70.62	70.54
	w. MedMAP (Δ)	69.12 (3.68 \uparrow)	78.29 (7.67 \uparrow)	72.84 (2.30 \uparrow)
BraTS2020	w.o. MedMAP	72.44	72.94	74.38
	w. MedMAP (Δ)	73.75 (1.31 \uparrow)	74.76 (6.76 \uparrow)	76.41 (0.38 \uparrow)

(%) [29] to evaluate the performance: higher Dice indicates better segmentation performance.

B. Implementation

For comparison fairness, we implant the proposed alignment paradigm to retrain each employed backbones [1], [15], [18] following identical respective experimental settings except the dataset configuration and the batch size, given by each author's released codes. The BraTS 2018 dataset is split into training, validation, and testing sets following Proto-KD [13], while the other BraTS 2020 dataset is used with three-fold cross-validations. In contrast to its official version, the batch size of mmFormer [18] is set to 1 and the batch size of PMKL [1] is set to 4 while the others remain the same. Models are implemented on one Nvidia GeForce RTX 3090Ti GPU with Pytorch.

VI. EXPERIMENT RESULTS

As discussed in Sec. II-A, recent approaches to predict annotations in the Missing Modality scenarios (MM) mainly include Knowledge Distillation (*e.g.* PMKL [1]), Shared Latent Space (*e.g.* mmFormer [18]), and Domain Adaption (*e.g.* ACN [15]). The proposed Alignment Paradigm will be implanted into the aforementioned recent SOTAs to evaluate the effectiveness. Specifically, Section VI-A will present statistical improvements given by the proposed MedMAP, measured by averaged dice as well as improvement (marked in red) and decline (in blue) in Table I. Details can also be found across various MM on both datasets in Table II. Sec. VI-B visualizes examples with and without P_{mix} . In Sec. VI-C, we compare several possible structures in key components of the proposed MedMAP, which guide us to find the most suitable encoder and anchor. In Sec. VI-D, the selection of hyperparameters will be introduced.

A. Quantitative Comparisons

1) Averaged results across prediction classes and MM:

As seen from Table I, we can conclude that the proposed MedMAP effectively promotes the prediction performance. Specifically, on the BraTS2018 dataset, it improves 3.68%, 7.67%, and 2.30% of the Dice Scores on PMKL, mmFormer, and ACN respectively. Improvements are 1.31%, 6.76%, and 0.38% of the Dice Scores on PMKL, mmFormer, and ACN respectively on the BraTS2020 dataset.

2) Performance improvement on different prediction classes:

In both Table II, the right-most columns of each dataset (Total Avg.) indicate the average performance across different MM. From them, we can identify when the proposed MedMAP is absent, the mmFormer achieves 83.67%, 73.04%, and 55.15%, respectively, on the BraTS2018 dataset, and 85.79%, 73.23%, and 59.81% on BraTS2020 when predicting WT, TC, and ET. Notably, on both datasets, predictions obtain lower dice scores on TC and ET than on the WT. The presence of the proposed MedMAP significantly promotes the degraded predictions of TC and ET by 4.97% and 11.72% respectively on BraTS2018, and 2.99% and 15.29% on BraTS2020. Moreover,

TABLE II: Comparison of dice scores when different modalities are missing on BraTS2018 and BraTS2020. ● represents present modalities. ○ displays missing modalities, while N denotes the number of them. Statistics in rows with + display achieved performance of the proposed paradigm, while those in rows of Δ evaluate performance difference brought by the proposed MedMAP paradigms. Statistics in columns titled by Avg. present average dice scores, while those in Total Avg. columns display average dice scores across different missing modality scenarios.

		BraTS2018						BraTS2020									
Type	Flair T1 T1ce T2	○	○	○	●	○	Avg. N=2	Avg. N=1	Total Avg.	○	○	○	●	○	Avg. N=2	Avg. N=1	Total Avg.
WT	PMKL	81.00	70.50	73.31	84.11		76.72	78.10	77.32	82.79	75.76	76.92	86.19		84.17	87.67	83.75
	+ MedMAP	83.77	75.97	72.04	85.70		81.35	83.85	81.06	84.23	77.03	76.85	86.79		85.44	88.06	84.74
	Δ	2.77	5.47	-1.27	1.59		4.63	5.75	3.73	1.44	1.27	-0.07	0.60		1.27	0.89	0.99
	mmFormer	84.09	72.85	73.37	85.60		85.26	87.81	83.67	85.78	76.46	76.35	87.80		87.81	89.15	85.79
	+ MedMAP	85.32	85.50	85.71	84.51		86.61	86.97	86.26	87.46	87.74	87.51	87.77		87.86	87.96	87.79
	Δ	1.23	12.65	12.34	-1.09		1.35	-0.83	2.59	1.68	11.28	11.16	-0.03		0.07	-1.79	2.00
ACN		84.18	77.31	73.63	84.77		82.68	85.04	82.38	86.94	78.15	78.58	87.33		86.99	88.98	85.74
	+ MedMAP	86.68	78.09	79.31	87.66		83.98	85.25	83.95	86.57	78.91	78.56	87.54		86.98	88.77	85.98
	Δ	2.50	0.78	5.68	2.89		1.30	0.21	1.57	-0.37	0.76	-0.02	0.21		-0.01	-0.21	0.24
TC	PMKL	67.92	76.92	64.26	62.21		66.00	68.96	66.60	71.50	82.37	69.39	67.10		75.27	79.49	74.85
	+ MedMAP	69.91	80.35	68.39	68.44		68.14	74.24	69.83	71.78	82.48	71.63	69.98		77.05	81.05	76.13
	Δ	1.99	3.43	4.13	6.23		2.14	5.28	3.23	0.38	0.11	2.24	1.22		1.78	1.56	1.18
	mmFormer	67.80	77.32	64.56	64.08		75.01	78.99	73.04	71.03	81.06	68.77	72.14		79.12	82.69	73.23
	+ MedMAP	77.76	77.34	76.63	76.29		78.46	78.72	78.02	82.35	81.92	71.49	81.99		82.33	82.89	76.22
	Δ	9.96	0.02	12.07	12.21		3.44	-0.27	4.97	11.32	0.86	2.72	9.85		3.21	0.20	2.99
ACN		72.08	66.17	59.74	73.26		71.96	71.17	72.57	75.21	71.95	67.21	76.43		77.34	80.82	76.64
	+ MedMAP	74.41	70.42	67.13	76.74		73.79	76.90	73.49	75.76	70.46	67.26	76.92		76.88	81.03	76.96
	Δ	2.33	4.25	7.39	3.48		1.83	0.15	2.32	0.55	-0.49	0.05	0.49		-0.46	0.22	0.32
ET	PMKL	47.09	75.54	41.37	41.35		52.52	60.70	52.39	44.37	74.19	44.52	44.57		61.74	70.91	58.73
	+ MedMAP	45.17	76.44	47.66	43.57		56.86	69.27	56.47	48.17	76.64	44.82	49.02		62.68	70.44	60.38
	Δ	-1.92	0.90	6.29	2.22		4.34	8.57	4.09	3.80	2.45	0.30	4.45		0.94	-0.47	1.65
	mmFormer	40.08	72.19	38.89	37.23		58.05	68.44	55.15	46.30	75.42	43.80	44.26		63.04	71.46	59.81
	+ MedMAP	69.02	70.55	70.77	70.23		70.72	70.93	70.58	75.00	74.83	74.67	74.30		75.59	75.60	75.10
	Δ	28.94	-1.64	31.88	33.00		15.43	2.49	11.72	28.70	-0.59	30.87	30.04		12.55	4.14	15.29
ACN		47.79	75.60	43.25	42.21		58.79	66.55	56.66	49.27	77.55	46.65	46.70		63.38	71.19	60.77
	+ MedMAP	47.93	78.03	50.64	46.61		65.17	67.07	61.09	48.91	78.27	48.34	47.94		64.79	71.80	61.35
	Δ	0.14	2.43	7.39	4.40		6.39	0.52	4.43	-0.26	0.62	1.69	1.24		1.41	0.61	0.58

such achievement can also be identified in the mmFormer predictions on the WT by 2.59% and 2.00% respectively on both involved datasets.

Furthermore, the proposed MedMAP also boosts the performance of the other two backbones. Specifically, it improves PMKL by 3.73%, 3.23%, and 4.09% respectively on WT, TC, and ET of BraTS2018, and 0.99%, 1.18%, and 1.65% on BraTS2020. It improves ACN by 1.57%, 2.32%, and 4.43% on BraTS2018, as well as 0.24%, 0.32%, and 0.58% on BraTS2020.

3) *MedMAP improvement in different MM*: Since there are four modalities in each of the BraTS2018 and BraTS2020 datasets, there are in total $2^4 - 1 = 15$ possible MM. We will evaluate each of them in Table II. Columns in the tables are categorized and split by the number of MM apart from the right-most column: sub-columns from the left to the right contain results when N of the available four modalities are absent, where $N \in [3, 2, 1]$. When $N = 1$, all the detailed results are shown and when $N = 2$ and $N = 3$, the average results are shown. Although there are some slight decreases when adding our MedMAP, the improvement can be seen in most scenarios.

B. Qualitative Comparison

We can observe from Fig. 4 that in general, the performance of the model with P_{mix} is superior to that without it. When

comparing the first and second rows, as well as the first two columns of the third row (cases with three or two missing modalities), we find that the model without P_{mix} struggles to predict NCR/NET, with instances of both missed detections and false detections. Upon observing the predictions of the first and fourth rows, we observe that the model with P_{mix} demonstrates greater accuracy in predicting ED, with smoother ED edges and the ability to predict details. In conclusion, in cases with N modalities missing, the model with P_{mix} performs consistently better.

C. Comparison of Alignment Paradigm components

As part of the proposed MedMAP with an encoder and an aligning anchor, we conduct ablation studies to evaluate the effectiveness of both components. Regarding the encoder, we compare the enhanced and the non-shared encoder. For the anchor P_{mix} , we compare the proposed P_{mix} with the standard normal distribution [30]. Furthermore, we assess two different P_{mix} options namely P_{mix}^k and P_{mix}^* .

1) *Encoder*: As discussed in Sec. IV-A, the proposed alignment paradigm will only be possible when latent features are placed in the same space, by using some encoding architectures. In this sense, we would like to evaluate the prediction performance based on two different encoder configurations: the non-shared encoder and the enhanced encoder, termed as non-shared \mathcal{T} and \mathcal{T}^* , respectively. In non-shared \mathcal{T} , an

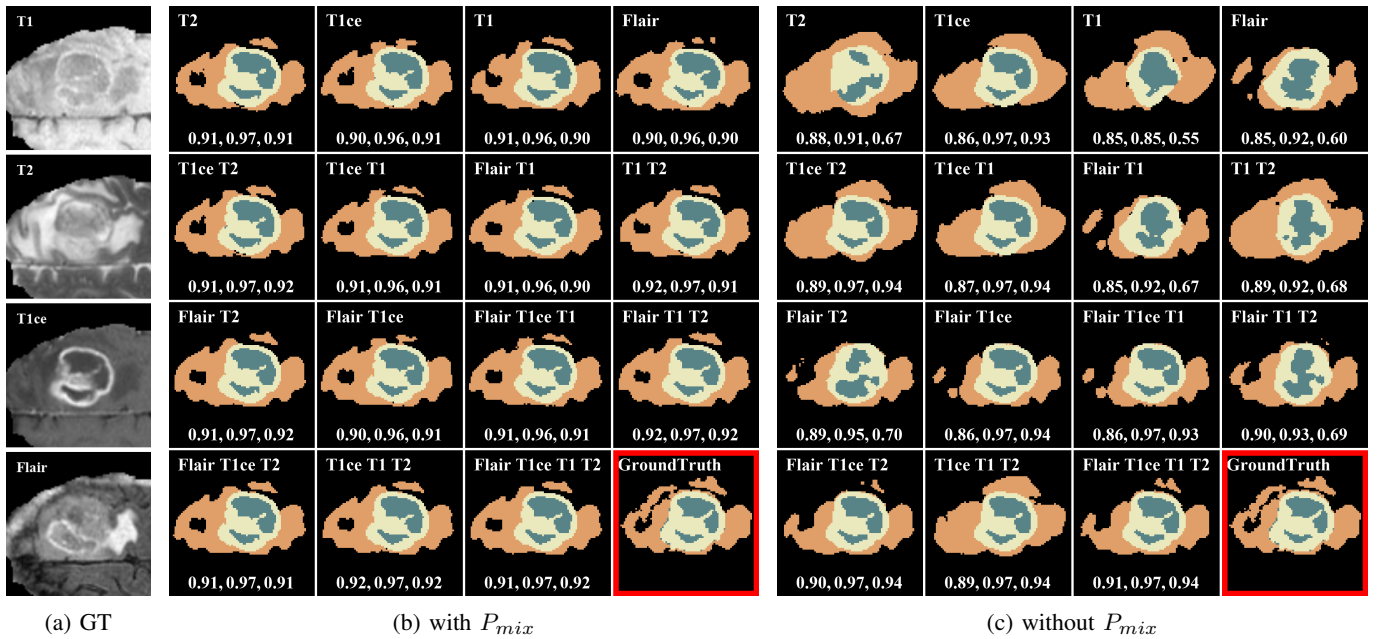


Fig. 4: Qualitative segmentation results of mmFormer with P_{mix} and without P_{mix} on BraTS2018 under all missing scenarios. Below each sub-figure is the Dice. The Dice texts from left to right are WT, TC, and ET. Different colors represent different organs: Blue: NCR/NET, Orange: ED, and Yellow: ET. Captions on the upper-left corners indicate present modalities. Bottom-right corner is the groundtruth labels.

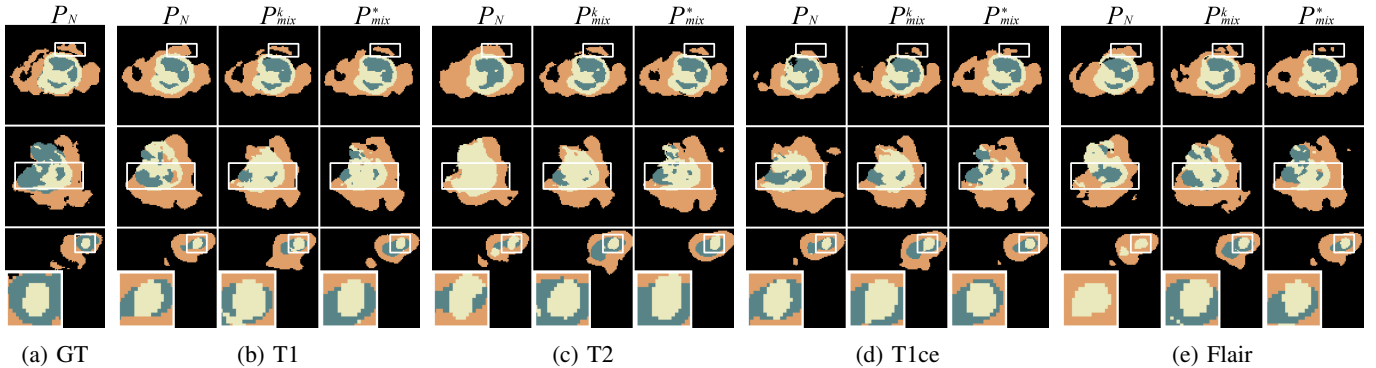


Fig. 5: Qualitative segmentation results of mmFormer with P_N , P_{mix}^k and P_{mix}^* on BraTS2018 where three modalities are missing.

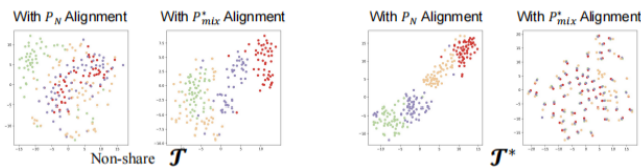


Fig. 6: T-SNE visualization of different anchors and encoders. Different colors mean different modalities.

independent encoder will be used to process each modality and channelized individually. Consequently, with J modalities, there will be J individual encoders. The total number of channels for the non-shared \mathcal{T} is $J \cdot c$, where c represents the number of channels of the input feature in one modality. The number of channels of \mathcal{T}^* is set to be $J \cdot c$ for fair comparison given an equivalent amount of training weights.

To examine closer the potential difference obtained, we evaluate the simplest involved backbone PMKL [1] based on U-Net architecture [31], and in the most challenging testing scenario when three over four in BraTS2018 modalities are missing. As such, the simplest model is sensitive to the change in model structure and the change of the information amount received. Comparing the results are presented in Table III, we can find that incorporating non-shared \mathcal{T} achieves a slight improvement in each modality. Further gains on the average dice scores can be identified by introducing \mathcal{T}^* . Figure 6 illustrates t-SNE [32] embeddings, where we can find that incorporating \mathcal{T}^* is able to narrow gaps between modalities. Therefore, \mathcal{T}^* is chosen as an appropriate encoder.

2) Comparison with standard normal distribution: We will compare the prediction performance achieved by setting the anchor to P_N which is a standard normal distribution. In

TABLE III: Comparison results with different types of encoders. Best results are highlighted as **bold**.

Present Modality	WT	TC	EC	Average	Avg.	\mathcal{T}
T1	73.31	64.26	41.37	58.98	65.30	without \mathcal{T}
T2	81.00	67.92	47.09	65.34		
T1ce	70.50	76.92	75.54	74.32		
Flair	84.11	62.21	41.35	62.56		
T1	72.99	63.28	38.92	58.40	65.72	non-share \mathcal{T}
T2	81.11	68.40	45.99	65.17		
T1ce	74.51	78.99	73.85	75.78		
Flair	83.98	67.10	39.48	63.52		
T1	75.50	65.98	40.09	60.53	66.40	\mathcal{T}^*
T2	82.68	67.14	44.82	64.88		
T1ce	74.00	78.64	72.71	75.12		
Flair	84.74	67.07	43.42	65.07		

TABLE IV: Comparison of segmentation results in each class and average dice scores with different anchor P_{mix} s.

Method	with P_N				with P_{mix}^k				with P_{mix}^*				Modality
	WT	TC	EC	Avg.	WT	TC	EC	Avg.	WT	TC	EC	Avg.	
Teachers	84.14	77.44	74.82	79.13	86.34	79.75	76.91	81.00	86.81	79.22	77.85	81.29	Full
PMKL [33]	75.60	65.59	43.31	61.50	75.06	66.80	41.43	61.10	72.04	68.39	47.66	62.70	T1
mmFormer [18]	83.86	75.70	65.94	75.17	84.83	76.80	68.87	76.83	85.71	76.63	70.77	77.70	
ACN [15]	74.52	61.65	45.99	60.72	74.95	66.32	45.82	62.36	79.31	67.13	50.64	65.69	
PMKL [33]	80.46	69.06	48.38	65.97	82.47	69.56	45.78	65.94	83.77	69.91	45.17	66.28	T2
mmFormer [18]	80.34	69.94	52.79	67.69	84.37	76.26	69.29	76.64	85.32	77.76	69.02	77.37	
ACN [15]	85.01	71.23	47.39	67.88	86.57	74.65	48.27	69.83	86.68	74.41	47.93	69.67	
PMKL [33]	73.89	80.86	77.48	77.41	77.46	80.71	75.40	77.86	75.97	80.35	76.44	77.58	T1ce
mmFormer [18]	82.23	76.32	67.70	75.42	83.68	76.09	69.81	76.53	85.50	77.34	70.55	77.80	
ACN [15]	77.86	67.07	77.63	74.19	78.07	70.05	76.73	74.95	78.09	70.42	78.03	75.51	
PMKL [33]	84.09	66.78	42.13	64.33	83.84	68.89	41.41	64.71	85.70	68.44	43.57	65.90	Flair
mmFormer [18]	80.45	70.50	54.25	68.40	83.90	76.05	65.55	75.17	84.51	76.29	70.23	77.01	
ACN [15]	85.01	71.23	47.39	67.88	87.16	77.06	46.08	70.10	87.66	76.64	46.61	70.30	

particular, given J modalities, P_{mix} is achieved by minimizing $\mathbb{E}[2 \log 1/v(\mathbf{Z}_j^*) + v(\mathbf{Z}_j^*)^2 + (\bar{\mathbf{Z}}_j^*)^2/2 - 1/2]$, where $\bar{\mathbf{Z}}_j^*$ and $v(\mathbf{Z}_j^*)$ denote the mean and variance of \mathbf{Z}_j^* , which are optimized during training.

As for KD and DA, the performance achieved by student models is dependent on the respective teacher models. Namely, a better teacher will probably provide better guidance to the respective student given the same architectures and knowledge distillation method. We will report the performance of both teachers and students. For SLS approaches, we only present the performance of the model itself. The first line of Table IV presents the results of teachers among anchors of P_N and P_{mix} s. They will be used to guide the downstream students by KD and DA approaches. Other lines of Table IV show the results obtained by students guided by KD, DA, as well as SLS methods across different anchors. It is evident that teachers with latent space aligned to P_{mix} exhibit better segmentation performance, with 81% and 81.29% dices of P_{mix} and 79.13% dice of P_N . Aligning to P_{mix} will also achieve superior performance than aligning to P_N .

The t-SNE [32] embeddings depicted in Figure 6 also demonstrate consistent finding when \mathcal{T}^* is applied, P_{mix} effectively aligns each modality together, as the distribution centers of each modality are almost overlapping. This indicates that the gaps between modalities are narrowed. However, when P_N is used as the anchor, the modality gaps are not sufficiently narrowed, failing to fill the space adequately. Furthermore, in reference with Figure 5, it is observed that models with P_{mix} perform better than those with P_N .

3) P_{mix}^k and P_{mix}^* : In Sec. IV-A, P_{mix}^k describes the latent space distribution of a specific modality and P_{mix}^* is a weighted combination of all modalities. We present comparison results when only one modality is available in Table IV. Clearly, we can observe that the model with P_{mix}^* achieves better prediction performance than that obtained by P_{mix}^k . Figure 5 displays segmentation visualization examples, where we can observe that P_{mix}^* consistently obtains the most superior prediction performance among all other anchors.

D. Ablation Studies of Hyperparameters

1) *Initialization of P_{mix}^** : As discussed in Sec. IV-A.2, initialization of w_j is crucial for the convergence in optimizing the model. Since P_{mix}^* is an adaptive version of P_{mix}^k , we utilize some prior knowledge from P_{mix}^k to initialize the parameter. Particularly, in this paper, we set the initialization weight for T1, T2, T1ce, and Flair to be 0, 0, 0, and 1 respectively.

2) *Parameter of alignment weight*: We have found that the alignment loss is not sensitive to the hyperparameter. In this paper, we empirically set the alignment loss to one-eighth of the original loss.

VII. CONCLUSION

In this paper, we present a novel Medical Modality Alignment Paradigm to mitigate the modality gaps whilst learning simultaneously invariant feature representations in segmenting brain tumors with missing modalities. Specifically, we invent an alignment paradigm for the models with an encoder encouraging that all modalities are in the same space and a latent space distribution P_{mix}^* as the aligning anchor. Meanwhile, we provide theoretical support for the proposed alignment paradigm, demonstrating that individual alignment of each modality to P_{mix} certifies a tighter evidence lower bound than mapping all modalities as a whole. Extensive experiments have demonstrated the superiority of the proposed paradigm over several latest state-of-the-art approaches, enabling better segment the brain tumor with missing modalities.

REFERENCES

- [1] C. Chen, Q. Dou, Y. Jin, Q. Liu, and P. A. Heng, "Learning with privileged multimodal knowledge for unimodal segmentation," *IEEE transactions on medical imaging*, vol. 41, no. 3, pp. 621–632, 2021.
- [2] Z. Zhao, H. Yang, and J. Sun, "Modality-adaptive feature interaction for brain tumor segmentation with missing modalities," in *International Conference on Medical Image Computing and Computer-Assisted Intervention*. Springer, 2022, pp. 183–192.
- [3] T. Lindig, R. Kotikalapudi, D. Schweikardt, P. Martin, F. Bender, U. Klose, U. Ernemann, N. K. Focke, and B. Bender, "Evaluation of multimodal segmentation based on 3d t1-, t2- and flair-weighted images—the difficulty of choosing," *Neuroimage*, vol. 170, pp. 210–221, 2018.
- [4] B. H. Menze, A. Jakab, S. Bauer, J. Kalpathy-Cramer, K. Farahani, J. Kirby, Y. Burren, N. Porz, J. Slotboom, R. Wiest *et al.*, "The multimodal brain tumor image segmentation benchmark (brats)," *IEEE transactions on medical imaging*, vol. 34, no. 10, pp. 1993–2024, 2014.
- [5] D. D. Patil and S. G. Deore, "Medical image segmentation: a review," *International Journal of Computer Science and Mobile Computing*, vol. 2, no. 1, pp. 22–27, 2013.
- [6] O. Maier, B. H. Menze, J. Von der Gabelntz, L. Häni, M. P. Heinrich, M. Liebrand, S. Winzeck, A. Basit, P. Bentley, L. Chen *et al.*, "Isles 2015—a public evaluation benchmark for ischemic stroke lesion segmentation from multispectral mri," *Medical image analysis*, vol. 35, pp. 250–269, 2017.

- [7] Y. Ding, X. Yu, and Y. Yang, "Rfnnet: Region-aware fusion network for incomplete multi-modal brain tumor segmentation," in *Proceedings of the IEEE/CVF international conference on computer vision*, 2021, pp. 3975–3984.
- [8] D. Chen, Y. Qiu, and Z. Wang, "Query re-training for modality-agnostic incomplete multi-modal brain tumor segmentation," in *International Conference on Medical Image Computing and Computer-Assisted Intervention*. Springer, 2023, pp. 135–146.
- [9] Y. Qiu, D. Chen, H. Yao, Y. Xu, and Z. Wang, "Scratch each other's back: Incomplete multi-modal brain tumor segmentation via category aware group self-support learning," in *Proceedings of the IEEE/CVF International Conference on Computer Vision*, 2023, pp. 21 317–21 326.
- [10] Y. Qiu, Z. Zhao, H. Yao, D. Chen, and Z. Wang, "Modal-aware visual prompting for incomplete multi-modal brain tumor segmentation," in *Proceedings of the 31st ACM International Conference on Multimedia*, 2023, pp. 3228–3239.
- [11] Y. Liu, L. Fan, C. Zhang, T. Zhou, Z. Xiao, L. Geng, and D. Shen, "Incomplete multi-modal representation learning for alzheimer's disease diagnosis," *Medical Image Analysis*, vol. 69, p. 101953, 2021.
- [12] M. Hu, M. Maillard, Y. Zhang, T. Ciceri, G. La Barbera, I. Bloch, and P. Gori, "Knowledge distillation from multi-modal to mono-modal segmentation networks," in *Medical Image Computing and Computer Assisted Intervention–MICCAI 2020: 23rd International Conference, Lima, Peru, October 4–8, 2020, Proceedings, Part I 23*. Springer, 2020, pp. 772–781.
- [13] S. Wang, Z. Yan, D. Zhang, H. Wei, Z. Li, and R. Li, "Prototype knowledge distillation for medical segmentation with missing modality," in *ICASSP 2023-2023 IEEE International Conference on Acoustics, Speech and Signal Processing (ICASSP)*. IEEE, 2023, pp. 1–5.
- [14] R. Azad, N. Khosravi, and D. Merhof, "Smu-net: Style matching u-net for brain tumor segmentation with missing modalities," in *International Conference on Medical Imaging with Deep Learning*. PMLR, 2022, pp. 48–62.
- [15] Y. Wang, Y. Zhang, Y. Liu, Z. Lin, J. Tian, C. Zhong, Z. Shi, J. Fan, and Z. He, "Acn: adversarial co-training network for brain tumor segmentation with missing modalities," in *Medical Image Computing and Computer Assisted Intervention–MICCAI 2021: 24th International Conference, Strasbourg, France, September 27–October 1, 2021, Proceedings, Part VII 24*. Springer, 2021, pp. 410–420.
- [16] M. Havaei, N. Guizard, N. Chapados, and Y. Bengio, "Hemis: Hetero-modal image segmentation," in *Medical Image Computing and Computer-Assisted Intervention–MICCAI 2016: 19th International Conference, Athens, Greece, October 17-21, 2016, Proceedings, Part II 19*. Springer, 2016, pp. 469–477.
- [17] T. Varsavsky, Z. Eaton-Rosen, C. H. Sudre, P. Nachev, and M. J. Cardoso, "Pimms: permutation invariant multi-modal segmentation," in *Deep Learning in Medical Image Analysis and Multimodal Learning for Clinical Decision Support: 4th International Workshop, DLMIA 2018, and 8th International Workshop, ML-CDS 2018, Held in Conjunction with MICCAI 2018, Granada, Spain, September 20, 2018, Proceedings 4*. Springer, 2018, pp. 201–209.
- [18] Y. Zhang, N. He, J. Yang, Y. Li, D. Wei, Y. Huang, Y. Zhang, Z. He, and Y. Zheng, "mmformer: Multimodal medical transformer for incomplete multimodal learning of brain tumor segmentation," in *International Conference on Medical Image Computing and Computer-Assisted Intervention*. Springer, 2022, pp. 107–117.
- [19] S. Choi, S. Jung, H. Yun, J. T. Kim, S. Kim, and J. Choo, "Robustnet: Improving domain generalization in urban-scene segmentation via instance selective whitening," in *Proceedings of the IEEE/CVF Conference on Computer Vision and Pattern Recognition*, 2021, pp. 11 580–11 590.
- [20] Z. Tan, X. Yang, and K. Huang, "Rethinking multi-domain generalization with a general learning objective," *arXiv preprint arXiv:2402.18853*, 2024.
- [21] M. Ma, J. Ren, L. Zhao, D. Testuggine, and X. Peng, "Are multi-modal transformers robust to missing modality?" in *Proceedings of the IEEE/CVF Conference on Computer Vision and Pattern Recognition*, 2022, pp. 18 177–18 186.
- [22] Y. Ganin, E. Ustinova, H. Ajakan, P. Germain, H. Larochelle, F. Laviolette, M. Marchand, and V. Lempitsky, "Domain-adversarial training of neural networks," *The journal of machine learning research*, vol. 17, no. 1, pp. 2096–2030, 2016.
- [23] Y. Li, X. Tian, M. Gong, Y. Liu, T. Liu, K. Zhang, and D. Tao, "Deep domain generalization via conditional invariant adversarial networks," in *Proceedings of the European conference on computer vision (ECCV)*, 2018, pp. 624–639.
- [24] Y. Li, M. Gong, X. Tian, T. Liu, and D. Tao, "Domain generalization via conditional invariant representations," in *Proceedings of the AAAI conference on artificial intelligence*, vol. 32, no. 1, 2018.
- [25] S. Hu, K. Zhang, Z. Chen, and L. Chan, "Domain generalization via multidomain discriminant analysis," in *Uncertainty in Artificial Intelligence*. PMLR, 2020, pp. 292–302.
- [26] S. M. Perlaza, G. Bisson, I. Esnaola, A. Jean-Marie, and S. Rini, "Empirical risk minimization with relative entropy regularization," *IEEE Transactions on Information Theory*, pp. 1–1, 2024.
- [27] S. Ben-David, J. Blitzer, K. Crammer, A. Kulesza, F. Pereira, and J. W. Vaughan, "A theory of learning from different domains," *Machine learning*, vol. 79, pp. 151–175, 2010.
- [28] S. Bakas, H. Akbari, A. Sotiras, M. Bilello, M. Rozycki, J. S. Kirby, J. B. Freymann, K. Farahani, and C. Davatzikos, "Advancing the cancer genome atlas glioma mri collections with expert segmentation labels and radiomic features," *Scientific data*, vol. 4, no. 1, pp. 1–13, 2017.
- [29] L. R. Dice, "Measures of the amount of ecologic association between species," *Ecology*, vol. 26, no. 3, pp. 297–302, 1945.
- [30] R. Dorent, S. Joutard, M. Modat, S. Ourselin, and T. Vercauteren, "Hetero-modal variational encoder-decoder for joint modality completion and segmentation," in *Medical Image Computing and Computer Assisted Intervention–MICCAI 2019: 22nd International Conference, Shenzhen, China, October 13–17, 2019, Proceedings, Part II 22*. Springer, 2019, pp. 74–82.
- [31] Ö. Çiçek, A. Abdulkadir, S. S. Lienkamp, T. Brox, and O. Ronneberger, "3d u-net: learning dense volumetric segmentation from sparse annotation," in *Medical Image Computing and Computer-Assisted Intervention–MICCAI 2016: 19th International Conference, Athens, Greece, October 17-21, 2016, Proceedings, Part II 19*. Springer, 2016, pp. 424–432.
- [32] L. Van der Maaten and G. Hinton, "Visualizing data using t-sne," *Journal of machine learning research*, vol. 9, no. 11, 2008.
- [33] L.-C. Chen, G. Papandreou, F. Schroff, and H. Adam, "Rethinking atrous convolution for semantic image segmentation," *arXiv preprint arXiv:1706.05587*, 2017.